

Bulk morphologies of polystyrene-*block*-polybutadiene-*block*-poly(*tert*-butyl methacrylate) triblock terpolymers



Tina I. Löbbling^a, Panu Hiekkataipale^b, Andreas Hanisch^a, Francesca Bennet^a,
Holger Schmalz^a, Olli Ikkala^b, André H. Gröschel^{b, **}, Axel H.E. Müller^{a, c, *}

^a Makromolekulare Chemie II, Universität Bayreuth, 95440 Bayreuth, Germany

^b Department of Applied Physics, Aalto University School of Science, 02150 Espoo, Finland

^c Institut für Organische Chemie, Johannes Gutenberg-Universität Mainz, D-55099 Mainz, Germany

ARTICLE INFO

Article history:

Received 28 November 2014

Received in revised form

9 February 2015

Accepted 14 February 2015

Available online 20 February 2015

Dedicated in friendship to Kris Matyjaszewski on the occasion of his 65th anniversary.

Keywords:

Phase diagram

Triblock terpolymers

Bulk morphologies

ABSTRACT

The self-assembly of block copolymers in the bulk phase enables the formation of complex nanostructures with sub 100 nm periodicities and long-range order, both relevant for nanotechnology applications. Here, we map the bulk phase behavior of polystyrene-*block*-polybutadiene-*block*-poly(*tert*-butyl methacrylate) (SBT) triblock terpolymers on a series of narrowly distributed polymers with widely different block volume fractions, ϕ_S , ϕ_B and ϕ_T . In dependence of ϕ , we find the lamella–lamella, core-shell cylinder, cylinder-in-lamella and core-shell gyroid morphology, but also a rarely observed cylinder-in-lamella phase. The bulk morphologies are thoroughly characterized by transmission electron microscopy (TEM) and small angle X-ray scattering (SAXS) and display unusually broad stability regions, i.e. morphologies are observed over a broad range of compositions. We attribute this phase behavior to the asymmetric distribution of block–block incompatibilities, along the SBT block sequence, which are relatively large for S/B and S/T interfaces, but small for B/T. The higher enthalpic penalties at the S/B and S/T interface cause B to preferentially spread on the T microdomain thereby adopting its geometry. The morphological behavior of SBT is thus dominated by the volume ratio of the end blocks, ϕ_S and ϕ_T , which reduces the number of potential morphologies to only a few, mostly the core-shell analogue of diblock copolymer morphologies. In general, a simplified terpolymer bulk behavior with large stability regions for morphologies offers straightforward synthetic targeting of specific morphologies that usually only appear in a small parameter space as demonstrated here on the core-shell gyroid.

© 2015 Elsevier Ltd. All rights reserved.

1. Introduction

Block copolymers consist of covalently linked polymer blocks with differences in physical or chemical properties. The resulting block–block incompatibility creates the conflict of short-range attraction and long-range repulsion that drives self-assembly of block copolymers into predictable bulk morphologies with nanometer periodicities. Important parameters that govern the

geometric arrangement of the phases are the volume fractions, ϕ_A (with $\phi_B = 1 - \phi_A$) of the participating blocks, A and B, and their block–block incompatibility, $\chi_{AB}N$, which is the Flory–Huggins–interaction parameter χ_{AB} , multiplied by the number of monomer units (degree of polymerization), $N = N_A + N_B$ [1]. The microphase separation is the result of enthalpic (interfacial energy of the two blocks) and entropic (chain stretching) contributions and is well understood given the dedicated efforts of theoretical [2–4] and experimental characterization of bulk phase diagrams [5–8]. AB diblock copolymers can adopt a limited number of stable bulk morphologies depending on these parameters such as the sphere, cylinder, gyroid and lamellar morphology, often found in the strong segregation regime above the order–disorder transition [1]. Except synthetic control of morphology (block length and choice of monomers), there are several post polymerization methods to

* Corresponding author. Institut für Organische Chemie, Johannes Gutenberg-Universität Mainz, D-55099 Mainz, Germany.

** Corresponding author.

E-mail addresses: andre.groschel@aalto.fi (A.H. Gröschel), axel.mueller@uni-mainz.de (A.H.E. Müller).

manipulate the phase behavior of diblock copolymers, e.g., by changing the volume fraction of one of the blocks *via* blending with homo- and copolymers [9,10], nanoparticles [11] or *via* hydrogen bonding [12–15]. Also thermally induced order-order-transitions [16,17], shear alignment [18,19] and alignment in electrical fields [20–22] have evolved to state-of-the-art techniques to induce, alter and optimize long-range order or to switch between morphologies.

Compared to the straightforward phase behavior of diblock copolymers, ABC triblock terpolymers feature higher morphological complexity due to the increased number of interaction parameters, χ_{AB} , χ_{BC} , χ_{AC} , and volume fractions, ϕ_A , ϕ_B (with $\phi_C = 1 - \phi_A - \phi_B$) [23,24]. Three blocks further give rise to variation in architecture (linear or miktoarm stars) [25–27] and block sequence (ABC, BAC, CAB) [28,29]. Nowadays, the synthesis of tailor-made ABC triblock terpolymers (or multiblock copolymers) has become state-of-the-art through continuous progress and development of controlled/living radical and ionic polymerization techniques [30]. The increased number of participating blocks complicates the prediction of the bulk behavior, but also contributes to the tremendous variety and complexity of potential morphologies [31,32]. Stadler et al. pioneered studies on ABC triblock terpolymer self-assembly of polystyrene-*block*-polybutadiene-*block*-poly(methyl methacrylate) (SBM) in bulk. Besides the core-shell analogues of cylindrical and gyroid diblock copolymer morphologies, they identified many more complex block arrangements, e.g., the spheres-on-sphere, spheres-on-cylinder, helix-on-cylinder and a knitting pattern morphology, amongst others [33–35]. Since then, ternary phase diagrams of several triblock terpolymers (e.g. SBM, SVT, BVT; S = styrene, B = butadiene, M = methyl methacrylate, V = 2/4-vinylpyridine, T = *tert*-butyl methacrylate) have been thoroughly investigated and highlighted the vast morphological diversity [36–38]. These and other works demonstrate the impressive complexity of ABC triblock terpolymer bulk morphologies.

Block copolymer bulk morphologies found widespread interest as precisely nanostructured templating materials for applications ranging from catalysis [39–41], photovoltaics [42] and optics [43] to fuel cells and lithography [44–47]. The gyroid morphology is a triply periodic minimal surface [48] and attracts special attention as precursor in hybrid materials design for applications requiring high surface area and symmetry (e.g. solar cells [49] or nanofoams [50]). In this regard, ABC triblock terpolymers offer more sophisticated gyroid morphologies with either core-shell [51] or double gyroid configuration, i.e. two interconnected gyroid networks separated by a matrix. Especially in the latter case, separate loading of individual gyroid phases with metal precursors gives access to bimetallic interpenetrating networks [52]. ABC triblock terpolymers that form A/C lamellar morphologies were also used for the preparation of Janus particles of diverse geometry (sphere, cylinder, disc) through crosslinking of the B middle block of lamella-sphere, lamella-cylinder and lamella-lamella bulk morphologies with subsequent redispersion of the cross-linked particles [53–56]. Polymer-based Janus particles show enhanced interfacial activity [57,58] as demonstrated by their application as interfacial stabilizers in emulsion polymerization [59], dispersants for carbon nanotubes [60] and compatibilizers for polymer blends [61,62]. Given the diversity of terpolymer morphologies, their full potential has certainly not been harnessed as of yet, and several other morphologies could be attractive in view of applications. However to predict and reliably target specific morphologies also requires a comprehensive understanding of the

parameters that control the bulk behavior for a given combination of blocks.

This work contributes to the understanding of the relationship between block volume fractions, block–block interactions, and the resulting bulk morphologies within the system polystyrene-*block*-polybutadiene-*block*-poly(*tert*-butyl methacrylate) (SBT). This block combination shows large differences in the segment–segment incompatibility of S/T ($\chi_{ST} = 0.025$ [63]) and B/T ($\chi_{BT} = 0.007$ [64]), causing the B phase to preferably spread on the T phase. Hence, the morphology that is formed is mostly guided by the two end blocks, leading to a decreased complexity of the phase behavior and to large stability regions of the single phases. The synthesized series of SBT triblock terpolymers with varying volume fractions, ϕ_S , ϕ_B and ϕ_T , cover a wide range of morphologies ranging from lamella–lamella to core-shell cylinder and core-shell gyroid morphology. Also a cylinder-in-lamella morphology was found, that was up to now only rarely reported. All bulk morphologies were characterized by transmission electron microscopy (TEM) and small angle X-ray scattering (SAXS). Stability regions for the various bulk morphologies are summarized in a ternary phase diagram. The functional SBT terpolymer offers post polymerization modifications, e.g., the possibility to fixate the bulk structure *via* cross-linking of the B phase or form pH-responsive metal coordination sites, poly(methacrylic acid), by deprotection of the T phase. This may be interesting if combined e.g. with the gyroid morphology to create pH responsive channels.

2. Experimental part

2.1. Materials

Sec-butyl lithium (*sec*-BuLi, 1.3 M solution in cyclohexane/hexane: 92:8, Acros) was used without further purification. THF (p.a., Aldrich) was distilled from CaH₂ and K under dry N₂ atmosphere. 1,1-Diphenyl-ethylene (Aldrich) was distilled from *sec*-BuLi under reduced pressure. Styrene was degassed with three freeze-pump-thaw cycles followed by the addition of 1 mL di-*n*-butylmagnesium (1.0 M solution in heptane, Aldrich) per 10 mL monomer. After evaporation of heptane and stirring for 1 h, the desired amount of monomer was condensed into a glass ampule and stored in liquid nitrogen under nitrogen atmosphere until use. Gaseous 1,3-butadiene (Messer–Griesheim) was passed through columns filled with molecular sieves (4 Å) and basic aluminum oxide. Afterwards, it was condensed into a glass reactor and stirred over di-*n*-butylmagnesium at least two days prior to use. *Tert*-butyl methacrylate (*t*BMA, Aldrich) was first degassed with three freeze-pump-thaw cycles. After addition of tri-*n*-octylaluminum (25 wt.-% in hexanes, Aldrich) until a slight yellow color occurred, hexane was evaporated under reduced pressure and the mixture was stirred for 1 h before the monomer was condensed into a glass ampule and stored in liquid nitrogen under nitrogen atmosphere until use.

2.2. Synthesis of SBT triblock terpolymers

All SBT triblock terpolymers were synthesized *via* living anionic polymerization in THF at low temperatures according to a previous publication [65]. *Sec*-BuLi followed by styrene was added to THF at –70 °C. After the reaction was completed an aliquot of the precursor was taken for SEC analysis before 1,3-butadiene was added. The reaction mixture was heated to –10 °C and stirred for 6.5 h to ensure complete polymerization. The reaction mixture was cooled

Table 1
Characteristics of the used SBT triblock terpolymers.

Polymer ^a	M _w [kg/mol] ^b	PDI ^c	φ _S :φ _B :φ _T ^d	Bulk Morphology ^e
S ₃₁ B ₁₇ T ₅₂	108	1.09	0.30:0.18:0.52	LL
S ₃₆ B ₂₀ T ₄₄	148	1.12	0.35:0.21:0.44	LL
S ₃₈ B ₂₁ T ₄₁	140	1.10	0.37:0.22:0.41	LL
S ₄₀ B ₂₂ T ₃₈	132	1.06	0.39:0.23:0.38	LL
S ₆₆ B ₁₁ T ₂₃	85	1.03	0.65:0.12:0.23	CYL
S ₅₁ B ₂₈ T ₂₁	104	1.07	0.49:0.30:0.21	CYL
S ₇₂ B ₁₂ T ₁₆	78	1.03	0.71:0.13:0.16	CYL
S ₄₆ B ₄₁ T ₁₃	69	1.03	0.44:0.43:0.13	CL
S ₃₉ B ₅₁ T ₁₀	80	1.08	0.37:0.53:0.10	CL
S ₅₆ B ₃₇ T ₇	57	1.07	0.54:0.39:0.07	CL
S ₅₀ B ₄₅ T ₅	64	1.04	0.48:0.47:0.05	CL
S ₃₃ B ₄₃ T ₂₄	94	1.10	0.31:0.45:0.24	L/GYR
S ₅₀ B ₃₂ T ₁₈	64	1.04	0.48:0.34:0.18	GYR
S ₃₆ B ₄₇ T ₁₇	87	1.09	0.34:0.49:0.17	GYR
S ₄₅ B ₄₀ T ₁₅	71	1.04	0.43:0.42:0.15	GYR
S ₅₃ B ₃₄ T ₁₃	61	1.03	0.51:0.36:0.13	GYR

^a Subscripts denote the weight fractions of the corresponding blocks in % determined by ¹H-NMR.

^b Overall molecular weight determined by a combination of SEC and ¹H-NMR.

^c Determined via THF-SEC using PS standards.

^d Volume fractions of the corresponding blocks were calculated from the composition of the polymer using the density of the blocks according to Equation (1).

^e Determined with TEM and SAXS measurements: CYL = core-shell cylinder; GYR = core-shell gyroid; LL = lamella–lamella; CL = cylinder-in-lamella.

to $-50\text{ }^{\circ}\text{C}$ before a 6-fold molar excess (compared to *sec*-BuLi) of 1,1-diphenyl-ethylene was added. After stirring for 1 h an aliquot of the diblock precursor was taken for SEC analysis. Then, *t*BMA monomer was added at $-70\text{ }^{\circ}\text{C}$ and the reaction was heated to $-50\text{ }^{\circ}\text{C}$ for 2 h. During the polymerization of the *Pt*BMA block, larger amounts were taken at specific reaction times (monomer conversion was monitored with online FT-NIR spectroscopy) by direct precipitation into degassed methanol. After complete monomer consumption, 2 mL of degassed methanol were added to the polymer solution to terminate the still living chain ends. The characteristics of the synthesized polymers are summarized in Table 1.

The volume fractions of the blocks in Table 1 were calculated from the degree of polymerization (*N*) and the molar volume of the respective monomer unit (*V_m*) as exemplified for the S block in Equation (1):

$$\phi_S = \frac{N_S V_{m,S}}{(N_S V_{m,S} + N_B V_{m,B} + N_T V_{m,T})} \quad (1)$$

with $V_{m,S} = 99.0\text{ cm}^3/\text{mol}$, $V_{m,B} = 56.0\text{ cm}^3/\text{mol}$, and $V_{m,T} = 139.4\text{ cm}^3/\text{mol}$ calculated from the molecular weight of the monomers and their respective densities, $\rho_S = 1.04\text{ g/cm}^3$, $\rho_B = 0.96\text{ g/cm}^3$ and $\rho_T = 1.02\text{ g/cm}^3$ [66,67].

2.3. Preparation of bulk films

All SBT triblock terpolymer bulk films were prepared the same way. For that purpose, 100 mg of the polymer was dissolved in 2 mL THF to give a concentration of $c = 50\text{ g/L}$. The polymer solution was cast into a 5 mL glass vial and the solvent was then allowed to evaporate slowly at room temperature over several days to yield the bulk film.

2.4. Transmission electron microscopy (TEM)

For TEM analysis, ultra-thin sections were cut from the polymer film with a Reichert-Jung Ultracut E equipped with a diamond knife

at temperatures below T_g of the PB block (90 K). TEM measurements were performed in bright-field mode on a Zeiss CEM 902 electron microscope operated at 80 kV. Prior to TEM imaging, the samples were stained with OsO₄ vapor for 3 h at room temperature to increase the contrast of the PB phase [68].

2.5. Online FT-NIR spectroscopy

A Nicolet Magna 560 FT-IR optical bench equipped with a white light source and a PbS detector was used to record the NIR spectra. Online monitoring was accomplished using a laboratory autoclave (Büchi) equipped with an all glass low-temperature immersion transmission probe (Hellma) with an optical path length of 10 mm and connected to the spectrometer via 2 m fiber-optical cables. The probe was fed through a port in the stainless steel top plate of the reactor and immersed into the reaction mixture [69,70].

2.6. Nuclear magnetic resonance spectroscopy (¹H-NMR)

¹H-NMR Spectra were recorded on a Bruker Ultrashield 300 machine with a 300 MHz operating frequency using deuterated chloroform as solvent.

2.7. Size exclusion chromatography (SEC)

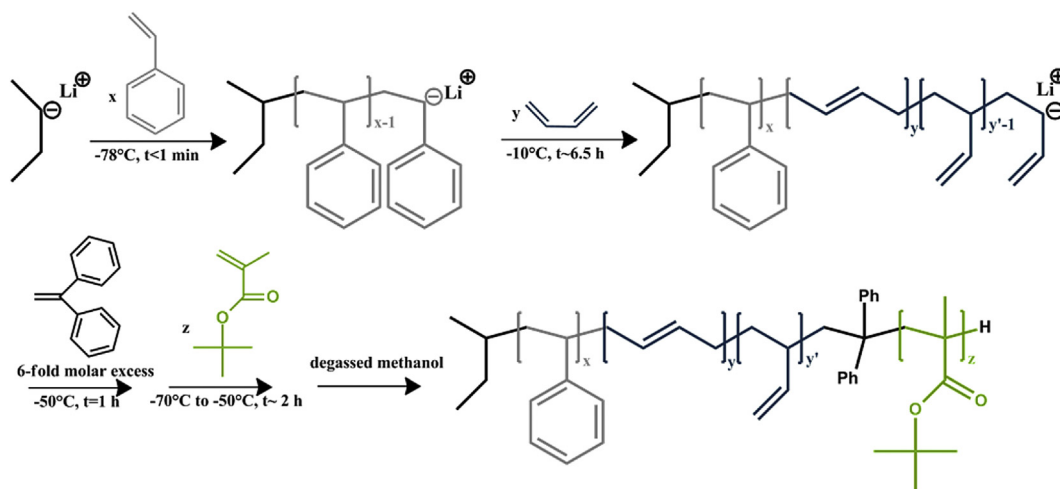
Size exclusion chromatography measurements were performed on a set of 30 cm SDV-gel columns of 5 μm particle size having a pore size of 10⁵, 10⁴, 10³, and 10² Å with refractive index and UV ($\lambda = 254\text{ nm}$) detection. SEC was measured at an elution rate of 1 mL/min with THF as eluent and applying a calibration with linear PS standards.

2.8. Small angle X-Ray scattering (SAXS)

Small angle X-ray scattering (SAXS) measurements of the films were performed in vacuum on a SAXS system, which includes a Bruker MICROSTAR rotating anode X-ray source with Montel collimating optics (CuK_α radiation $\lambda = 1.54\text{ \AA}$). The X-ray beam was further collimated using four sets of 4-blade slits (JJ X-Ray) and the diffraction pattern of the sample was collected on a 2-D area detector (Bruker Hi-Star). The distance of the detector was 3.5 m from the sample. One-dimensional SAXS data were obtained by azimuthally averaging the 2D scattering data. The magnitude of the scattering vector is given by $q = (4\pi\lambda^{-1})\sin\theta$, where 2θ is the scattering angle and to calibrate the *q*-range, silver behenate (AgBe) was used as a standard. The Lorentz correction was applied to correct the intensities of the X-ray scattering, where the intensities are reduced to zero at zero diffraction angle. The electron densities of the participating blocks are: $\rho_S = 0.566\text{ mol/cm}^3$, $\rho_B = 0.532\text{ mol/cm}^3$ and $\rho_T = 0.561\text{ mol/cm}^3$ [37,38]. Due to the low electron density difference between S and T only a weak scattering contrast is expected.

3. Results and discussion

The synthetic process for the sequential living anionic polymerization of polystyrene-*block*-polybutadiene-*block*-poly(*tert*-butyl methacrylate) (SBT) is summarized in Scheme 1. For this study, we synthesized a total of 16 SBT triblock terpolymers with varying weight (and thus volume) fractions as listed in Table 1. We abbreviate the polymers with S_xB_yT_z^M throughout this manuscript, where the subscripts denote the weight fraction of each block in wt.-% (for easier comparison), and the superscript the weight-average molecular weight in kg/mol.



Scheme 1. Synthesis of SBT triblock terpolymers via sequential living anionic polymerization.

The monomer conversion was followed with FT-NIR spectroscopy. The solvent subtracted NIR-spectra for the polymerization of PB block in $S_{53}B_{34}T_{13}^{61k}$ at different reaction times are shown in Fig. 1a. The signal at $\nu = 6116 \text{ cm}^{-1}$ corresponds to the first overtone of the vinyl C–H stretching and decreases with increasing conversion. The inset shows the first-order kinetic plot for this polymerization, where the conversion x_p was calculated according to Equation (2) with A_0 as the initial absorbance, A_t the absorbance at a certain time and A_∞ the absorbance at 100% monomer conversion.

$$x_p = \frac{A_0 - A_t}{A_0 - A_\infty} \quad (2)$$

Fig. 1b shows SEC elution traces of the PS precursor polymer (grey), the PS-*b*-PB diblock copolymer (black) and the final PS-*b*-PB-*b*-PtBMA triblock terpolymer ($S_{53}B_{34}T_{13}^{61k}$ green). The final SBT polymer shows a narrow distribution with only minor traces of PS homopolymers due to termination of few chains during addition of the butadiene block. The complete shift of the trace maintaining peak shape after addition of tBMA suggests quantitative initiation of the third block.

The overall molecular weights were chosen to be larger than 50 kg/mol so that sufficiently high Flory–Huggins-interaction parameters drive microphase separation above the order-disorder transition. For the present SBT system, the χ -parameters for S/B and S/T are $\chi_{SB} = 0.061$ [71] and $\chi_{ST} = 0.025$ [63], respectively. For B/T a value of $\chi_{BT} = 0.007$ is estimated [64], but this value inherits uncertainty as calculations are solely based on solubility parameters. The volume fractions, ϕ_S , ϕ_B and ϕ_T , are calculated in Table 1 and used throughout the manuscript as a measure to border each morphology as well as to discuss morphological transitions.

In the following, we discuss the phase behavior of SBT triblock terpolymers and their self-assembly into four distinct morphologies. The last section then summarizes the stability regions of the observed bulk phases in a ternary phase diagram.

3.1. Lamella–Lamella (LL) morphology

SBT terpolymers with equal S and T volume fractions, $\phi_S \approx \phi_T$, result in the lamella–lamella bulk morphology as exemplified by

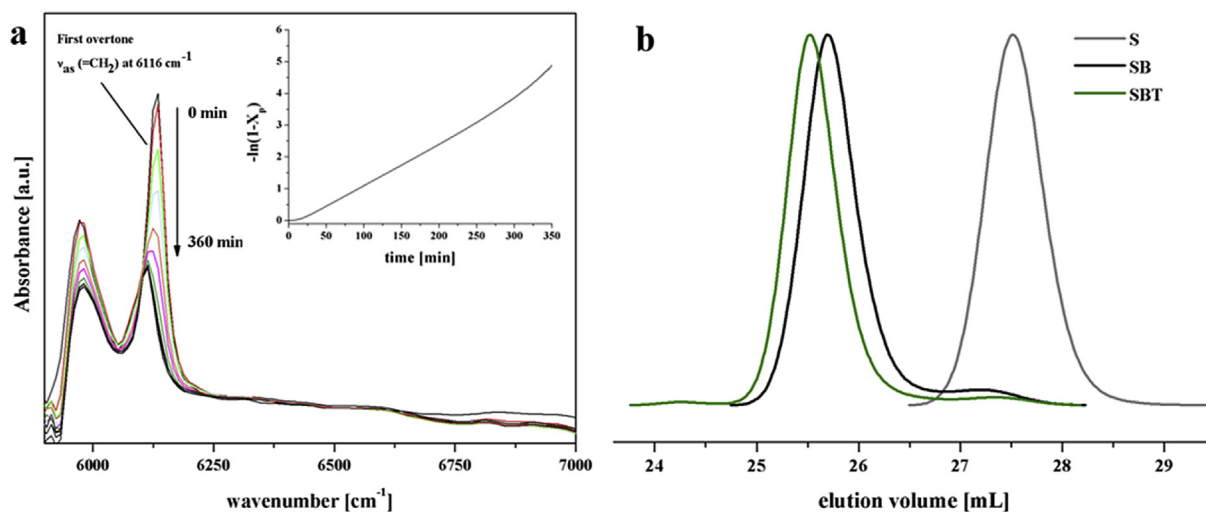


Fig. 1. Polymerization kinetics exemplified on the $S_{53}B_{34}T_{13}^{61k}$ triblock terpolymer. a) NIR-spectra of 1,3-butadiene polymerization in THF at -10°C after subtraction of the solvent background between $t = 0 \text{ min}$ and $t = 360 \text{ min}$. The inset shows the corresponding linear first order kinetic plot. b) SEC elution traces the PS precursor (grey), the PS-*b*-PB diblock copolymer (black) and the final PS-*b*-PB-*b*-PtBMA triblock terpolymer (green).

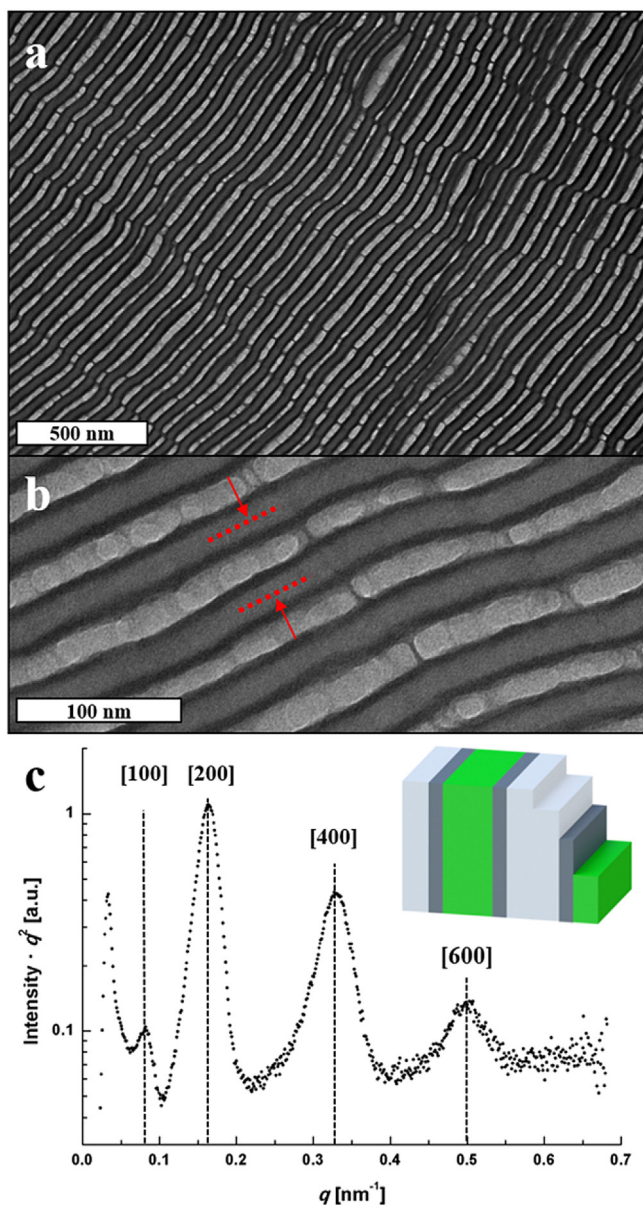


Fig. 2. Lamella–lamella morphology. a) TEM overview image and b) zoom-in of the $S_{40}B_{22}T_{38}^{132}$ bulk film cast from THF. OsO_4 staining renders S light grey and B dark grey, while T is not visible due to e -beam degradation. The red arrows in (b) mark the long period of the lamella–lamella morphology. c) Lorentz corrected SAXS pattern with characteristic reflexes for lamellar morphology. The schematic drawing represents the lamellar phases: S = light grey, B = dark grey, T = green.

the transmission electron microscopy (TEM) images of $S_{40}B_{22}T_{38}^{132}$ in Fig. 2. The sample was stained with OsO_4 , which covalently binds to the polybutadiene double bonds and increases the contrast of the B phase. In TEM, S appears light grey, B dark grey, and T bright due to e -beam degradation [72]. We determine a long period $L_0 = 68.3 \text{ nm} \pm 4.2 \text{ nm}$ as indicated by the red arrows in Fig. 2b. The thicknesses of the B and S lamellae are $d_{(B)} = 10.4 \text{ nm} \pm 1.6 \text{ nm}$ and $d_{(S)} = 23.9 \text{ nm} \pm 3.5 \text{ nm}$, respectively, whereas the disintegrating T lamella cannot be measured reliably in TEM image analysis. The schematic in

Fig. 2c shows the lamellar bulk morphology with S lamellae in light grey, B dark grey and T in green. Although one can easily identify the lamellar sequence in TEM, e -beam degradation of the T block leads to shrinkage of the T phase as well as deformation and wrinkling of the entire morphology. Arising shear forces during ultra-thin sectioning of the film add further uncertainty to the characterization based on TEM image analysis. Small-angle X-ray scattering (SAXS), on the other hand, is a non-invasive method and records distinct diffraction pattern from the sample. Fig. 2c shows a representative SAXS curve of $S_{40}B_{22}T_{38}^{132}$ with peaks at the relative positions 1: 2: 4: 6 corresponding to the [100], [200], [400] and [600] projections for a lamellar morphology. The [300] and [500] projections are missing or the intensity is within the range of the background noise of the spectra. This may be explained by the similar volume fractions, $\phi_S = 0.39$ and $\phi_T = 0.38$, and almost equal electron densities, $\rho_S = 0.566 \text{ mol/cm}^3$ and $\rho_T = 0.561 \text{ mol/cm}^3$. Thus, the relative maxima for lamellar spacing would appear at positions that are only half of the actual triblock terpolymer periodicity, i.e. comparable to the scattering curve of a “diblock copolymer”. Evaluation of the scattering curve maxima gives a long period of $L_0 = 76.6 \text{ nm} \pm 3.8 \text{ nm}$, which is slightly larger than the one obtained from TEM measurements ($L_0 = 68.3 \text{ nm} \pm 4.2 \text{ nm}$) due to the mentioned shrinkage of the T lamellae upon degradation. We obtain the LL morphology for various compositions covering a large range of B volume fractions from $\phi_B = 0.23$ – 0.18 (Table 1, entries 1–4) to only $\phi_B = 0.05$ for polymers in previous reports [55,73]. This behavior can be explained by comparing the χ -parameters. Since $\chi_{ST} > \chi_{BT}$, a B/T interface is more favored than S/T and considering also $\chi_{SB} > \chi_{BT}$, the B phase preferentially spreads on T. The asymmetry of χ -parameters between adjacent blocks has a crucial influence on the phase behavior and was also shown earlier by Stadler et al. for triblock terpolymers with post modification of blocks to induce a change of the χ -parameter [74]. In principle, B always engulfs the T phase, which in the special case of a T lamella (infinite expansion in one direction) then results in the observed B lamella even for low B volume fractions $\phi_B = 0.18$ and $\phi_B = 0.05$, where usually B cylinders and spheres are expected. We will address this unusual behavior in more detail also on the other morphologies.

3.2. Core-shell cylinder (CYL) morphology

For SBT triblock terpolymers with $\phi_S > \phi_T$, asymmetric end-blocks drive phase separation to the core-shell cylinder morphology (Table 1, entries 5–7). Exemplified on $S_{66}B_{11}T_{23}^{85}$ the TEM overview image shows long-range order core-shell cylinder morphology (Fig. 3a). The T cylinders arrange in a slightly distorted hexagonal lattice, wrapped by a B shell in an S matrix (Fig. 3a and b). The long-range order is further corroborated by the *fast Fourier transform* (FFT) pattern (Fig. 2a, inset). The angle of the unit cell is $\alpha = 81^\circ$ and $\beta = 99^\circ$ instead of $\alpha = 60^\circ$ and $\beta = 120^\circ$, and thus, the morphology displays a deformation that it is close to the orthorhombic core-shell cylinder morphology (see upper right corner of Fig. 3a).

The SAXS pattern (Fig. 3c) shows maxima at relative values of 1: $\sqrt{3}$: 2: $\sqrt{7}$ corresponding to typical [100], [110], [200], [210] indices for a hexagonally arranged cylinder morphology. A long period $L_0 = 52.5 \text{ nm} \pm 2.6 \text{ nm}$ was determined from SAXS measurements, which is slightly larger than the value $L_0 = 39.7 \pm 4.9 \text{ nm}$ obtained from TEM. As discussed before, this discrepancy may be explained through underlying inaccuracies in

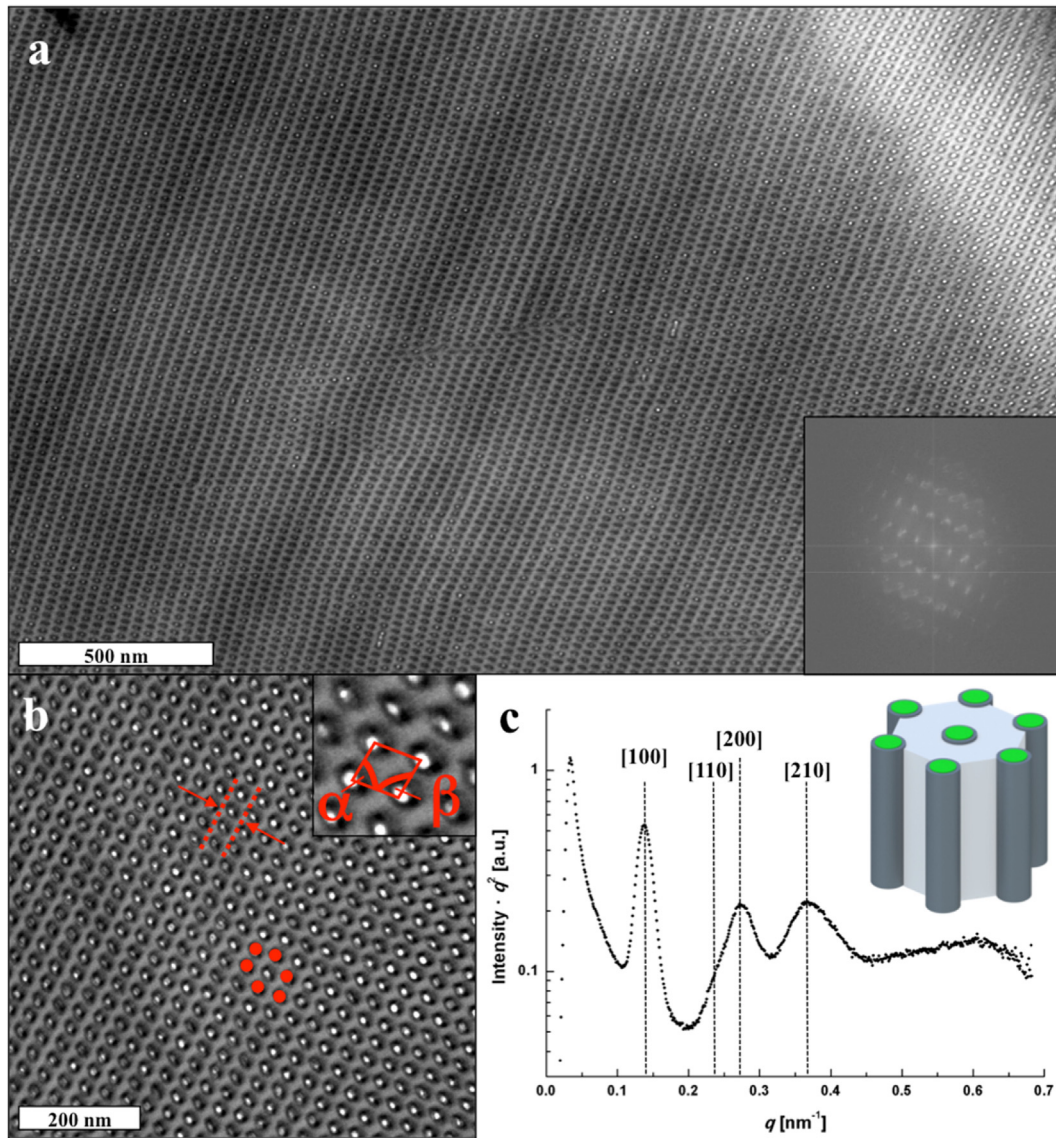


Fig. 3. Core-shell cylinder morphology. a) TEM overview image of $S_{66}B_{11}T_{23}^{85}$ bulk film cast from THF (inset shows FFT of (a)). b) Zoom-in on the core-shell morphology with red dots indicating the distorted hexagonal arrangement and red arrows mark the long period L_0 . TEM samples are stained with OsO_4 to enhance the contrast of B phase, which appears dark grey; S is light grey and T appears white due to e -beam degradation. The inset shows the angles α and β of the unit cell. c) The Lorentz corrected SAXS pattern shows reflections typical for hexagonal cylinder morphology. The inset shows a scheme of the morphology (S = light grey, B = dark grey, T = green).

determination of the long period by means of TEM such as shrinkage of the film as a result of e -beam degradation of T or deformation of the film during cutting. A diameter of $d_{c(S+B)} = 26.7 \pm 1.6$ nm for the core-shell cylinders was determined via TEM. This value cannot be measured with SAXS because this method only gives the long period of the entire structure. The SAXS data, the volume fractions of the blocks as well as TEM image analysis suggest core-shell cylinders with a T core and B shell embedded in an S matrix. The structure is illustrated in the inset of Fig. 3c. Although the B phase is relatively small with only $\phi_B = 0.12$, a homogeneous shell around the T cylinders is formed, which we explain in correspondence to the anomalies discussed for lamella–lamella morphology. The B

phase spreads onto T to prevent an S/T interface as a result of $\chi_{ST} > \chi_{BT}$. The cylindrical phase is observed even if the B content increases to $\phi_B = 0.30$ as in the case of $S_{51}B_{28}T_{21}^{94}$. In general, the B phase seems to engulf the T phase irrespective of its volume fraction and we find core-shell cylinders as long as the T block volume fraction remains $\phi_T < 0.25$. The spreading behavior of B suggests that the overall morphology is first and foremost governed by the volume fractions of the end blocks, S and T (especially for B as the minority phase). As long as the T block has a weight fraction corresponding to the cylinder morphology the B volume fraction can adopt a wide range of values without changing the morphology as it only spreads between S and T domains. Hence for SBT, the core-shell cylinder morphology has a

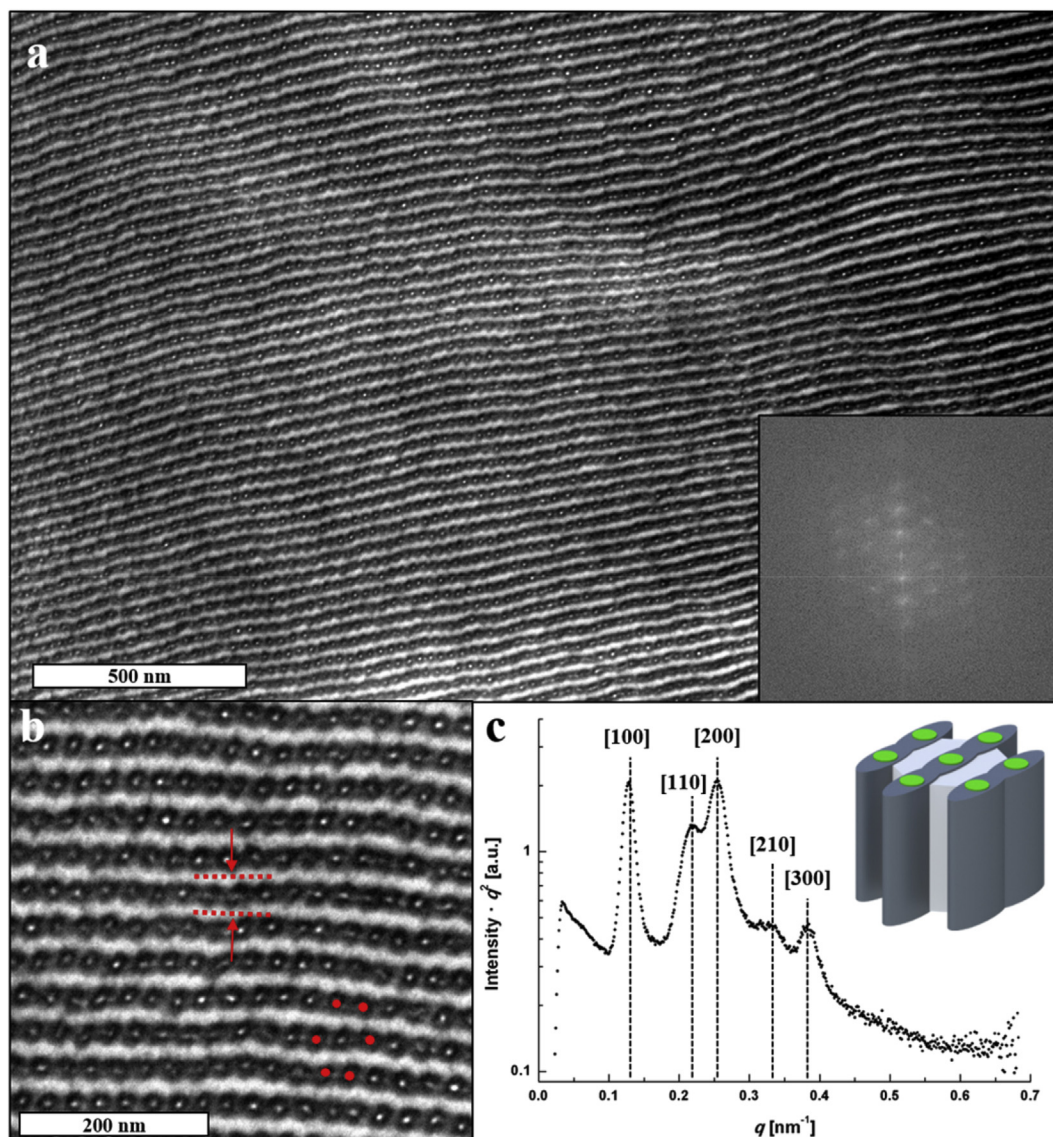


Fig. 4. Cylinder-in-lamella morphology. a) TEM overview with inset showing the FFT of this image and b) zoom-in on $S_{46}B_{41}T_{13}^{69}$ bulk film cast from THF. The B phase is stained with OsO_4 to enhance contrast (S is light grey and T appears white due to e -beam degradation). The S phase forms an undulated lamellar phase, while B lamellae contain T cylinders (red spots indicate hexagonal arrangement of T cylinders). The red arrows mark the long period L_0 . c) Lorentz corrected SAXS pattern show typical reflexes for lamellar and cylindrical morphologies. The schematic in c) shows the block arrangement for the cylinder-in-lamella morphology: S = light grey, B = dark grey, T = green.

high stability region. As shown earlier by Abetz et al. for high B content SBT terpolymers, also morphologies are observed with S and T being both spheres or both cylinders within the B matrix when the B phase increases to $\phi_B > 0.50$ [73]. In these cases, the B phase still separates S from T, which agrees with the assumptions drawn so far.

3.3. Cylinder-in-lamella (CL) morphology

For SBT triblock terpolymers with $\phi_S \gg \phi_T$ and simultaneously $\phi_B > 0.39$, we observe the formation of a morphology that is best described as hexagonally packed T cylinders exclusively located in B lamellae alternating with “empty” S lamellae. The TEM overview in Fig. 4a exemplifies this morphology on

$S_{46}B_{41}T_{13}^{69}$, where the light grey S phase forms continuous, undulated lamellae and the dark B lamellae accommodate white T cylinders. The T phase thereby still arranges in slightly distorted hexagonal long-range order as indicated by the FFT pattern and the red dots in Fig. 4b. The long period $L_0 = 38.5 \pm 1.7$ nm determined from TEM image analysis is small as compared to the previously discussed morphologies, which is expected given the rather low molecular weight of $M_w = 69$ kg/mol. The long period of $L_0 = 57.1 \text{ nm} \pm 2.9$ nm obtained from SAXS is again more reliable and larger than that from TEM. This morphology also has a relatively large stability region and is found for block compositions ranging from $\phi_T = 0.05$ – 0.13 , while $\phi_B > 0.39$ (Table 1, entries 8–11). This morphology was previously described for a block ter-/copolymer blend [75] and for polystyrene-*block*-

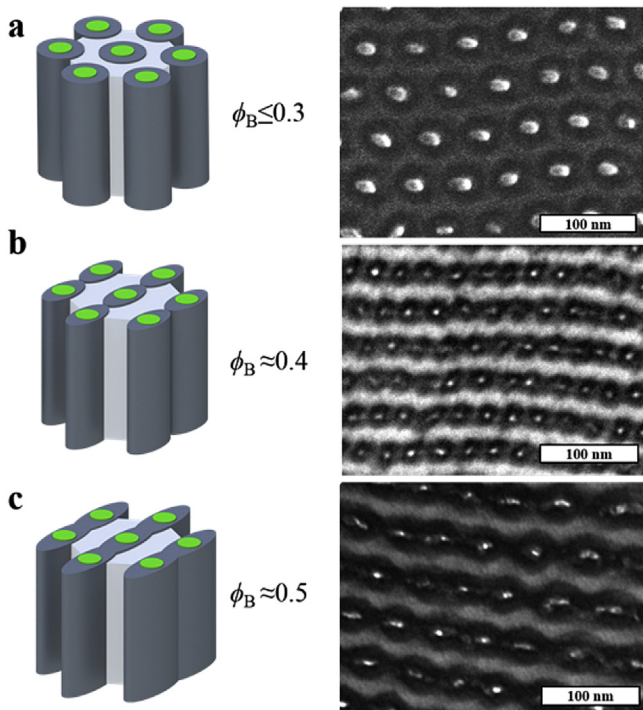


Fig. 5. Morphological evolution from core-shell cylinder to cylinder-in-lamella morphology. a) Core-shell cylinder morphology for volume fractions $\phi_B \leq 0.3$. The corresponding TEM image shows a bulk film of the $S_{51}B_{28}T_{21}^{104}$ triblock terpolymer. b) For $S_{46}B_{41}T_{13}^{69}$ with $\phi_B \approx 0.4$, the B shell becomes thicker (relative to T) developing connection points reminiscent of pearl-necklaces. c) Further increase to $\phi_B \approx 0.5$ leads to fusion of B into undulated lamellae incorporating T cylinders. The corresponding TEM image shows the $S_{39}B_{51}T_{10}^{80}$ bulk film (S = light grey, B = dark grey, T = green).

poly(2-vinylpyridine)-*block*-poly(*tert*-butyl methacrylate) [37], and denoted as undulated lamellae (UL). Although the S and B phases are clearly undulating, the UL terminology does not fully capture the complex geometrical arrangement of all phases. The SAXS pattern in Fig. 4c shows peaks at relative positions 1: $\sqrt{3}$: 2: $\sqrt{7}$: 3 and thus contains characteristics of both the lamella and the cylinder morphology, and is best described as cylinder-in-lamella (CL) morphology. TEM in combination with SAXS suggests the following block arrangement as according to the inset in Fig. 4c: as the minority phase, T (green) forms cylinders within the B lamellae phase (dark grey) alternating with continuous S lamellae (light grey).

Despite the seemingly complex positioning of the blocks, we can derive its origin rather easily with the help of our previous discussions. Fig. 5 illustrates the evolution from core-shell cylinders to cylinder-in-lamella morphology in dependence of the B volume fraction. First a core-shell morphology can be observed as long as the B volume fraction does not exceed $\phi_B = 0.30$ (Fig. 5a, Table 1, entry 6). The rather large $\phi_B = 0.3$ for $S_{51}B_{28}T_{21}^{104}$ in Fig. 5a still forms a continuous shell, yet already here the core and the shell of the cylinders experience a noticeable elliptic deformation in one direction. With increasing $\phi_B = 0.4$, the shell grows relative to the core and the high incompatibility χ_{SB} causes anisotropic deformation of the B shell. Similar to the core-shell cylinder morphology, we find hexagonally arranged T cylinders (Fig. 5b), yet with the

marked difference that the much larger B shells (in relation to T) start merging into a lamella. The overlapping B volume at $\phi_B = 0.5$ then fuses into a lamellar phase that incorporates the T cylinders (Fig. 5c). The hexagonal arrangement of the cylinders is thereby preserved.

3.4. Core-shell gyroid morphology

At a certain composition range, we identify the core-shell gyroid morphology in TEM and SAXS. In case of $S_{33}B_{43}T_{24}^{94}$ (Table 1, entry 12), a mixture of lamella–lamella and gyroid morphology was found, which changes to exclusive gyroid morphology upon decreasing the T volume fraction. Fig. 6a and b shows the TEM overview image of the $S_{53}B_{34}T_{13}^{61}$ bulk morphology as well as the zoom-in of most likely the [112] projection of the gyroid morphology [76]. From this projection a long period of $L_0 = 98.7 \pm 3.1$ nm was determined from TEM. Similar motifs that are characteristic for the core-shell gyroid morphology can also be found for SBT triblock terpolymers with compositions of $S_{45}B_{40}T_{15}^{71}$, $S_{36}B_{47}T_{17}^{87}$ and $S_{50}B_{32}T_{18}^{64}$ (Table 1, entries 13–16). This broad stability region of the gyroid is rather unusual for triblock terpolymers, but is again a consequence of the B phase that spreads as shell on the T gyroid, even at high $\phi_B = 0.35$ –0.50.

The SAXS pattern in Fig. 6c shows maxima at relative positions $\sqrt{3}$: $\sqrt{4}$: $\sqrt{7}$: $\sqrt{11}$: $\sqrt{13}$: $\sqrt{25}$: $\sqrt{35}$: $\sqrt{43}$ that are typical for the gyroid morphology, although peak broadening complicates indexing of all reflections [77]. The relative peak at $\sqrt{3}$ is assumed to correspond to the [211] direction. A long period of $L_0 = 106$ nm \pm 2 nm was determined from SAXS measurement and is in good agreement with TEM measurements. The inset in Fig. 5c shows a schematic drawing of the core-shell gyroid with S in light grey, B in dark grey and T in green. All measured gyroid samples have in common that T and B form the core-shell gyroid, which is embedded in an S matrix.

4. Phase diagram

Fig. 7 summarizes the discussed morphologies of SBT triblock terpolymers in a comprehensive ternary phase diagram. SBTs with the lowest volume fractions of the T block $\phi_T = 0.05$ –0.13 and high $\phi_B > 0.39$, phase separate to cylinder-in-lamella (CL, or undulated lamella) morphology (Fig. 6 orange area).

Asymmetric SBT triblock terpolymers with $\phi_S \geq 0.49$ and T fractions between $\phi_T = 0.15$ –0.25 form T core, B shell cylinders in S matrix (CYL, Fig. 6 blue area). When the S and B blocks are in the range of $\phi_S \approx \phi_B \approx 0.35$ –0.50 with T fractions of $\phi_T \approx 0.15$ the core-shell gyroid (GYR) morphology is present (Fig. 6 yellow area). The lamella–lamella (LL) phase (Fig. 6 green area) is observed in a rather large region including literature values (displayed as stars in the phase diagram) [55,73]. The large stability region is attributed to the fact that the B phase always spreads on T and forms lamellae as long as the S and T block are of similar volume fractions and form lamellae themselves ($\phi_S \approx \phi_T$). Due to $\chi_{ST} > \chi_{BT}$, the B phase tends to spread on T and complex morphologies such as sphere-on-cylinder, helix-on-cylinder or lamellar-sphere as observed for polystyrene-*block*-polybutadiene-*block*-poly(methyl methacrylate) (SBM) are absent [1]. The stability regions over relatively large block copolymer compositions simplify the phase behavior of SBT and the resultant morphologies are easier-to-target synthetically.

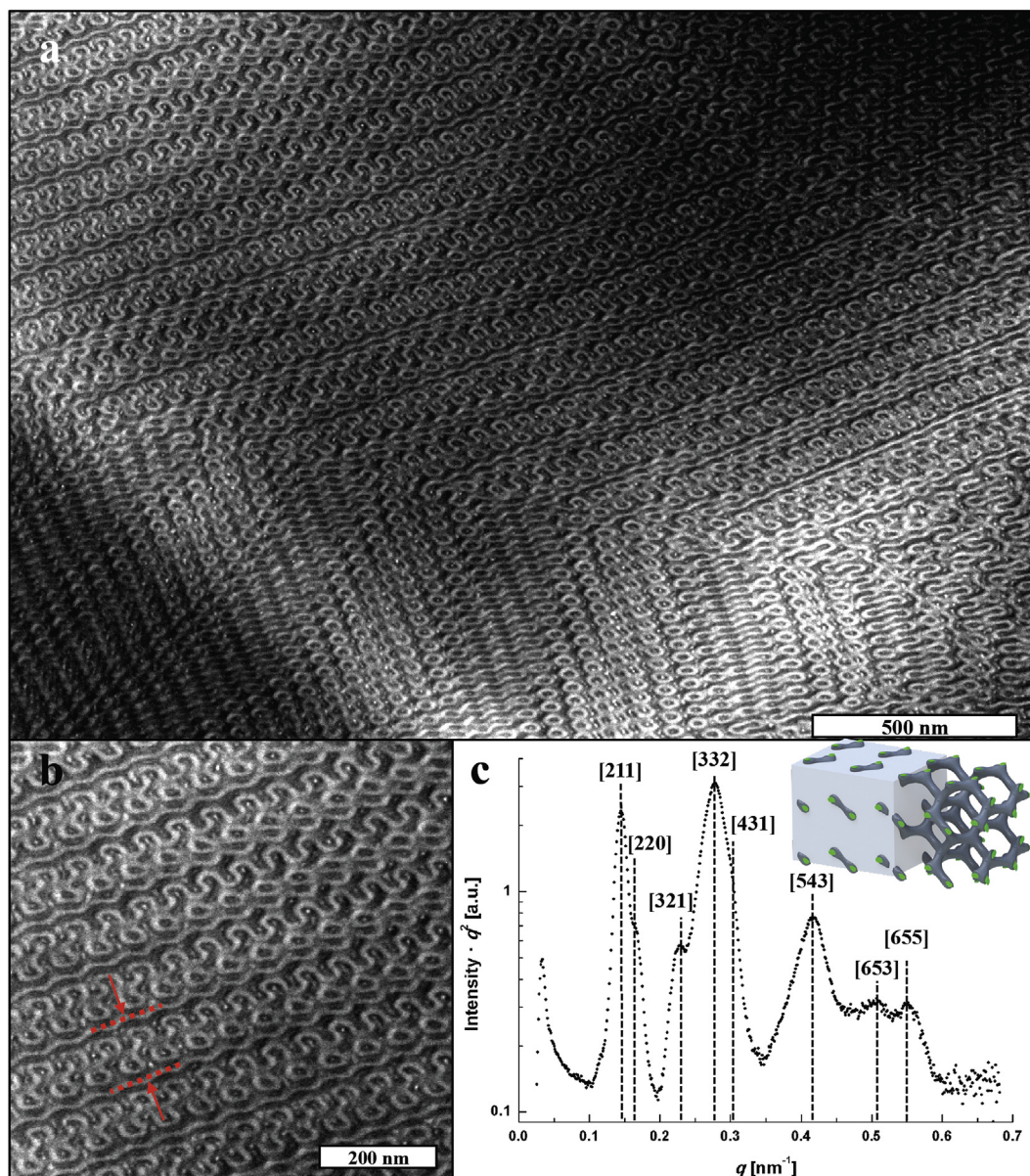


Fig. 6. Core-shell gyroid morphology. a) TEM overview and b) zoom-in of $S_{45}B_{40}T_{15}$ bulk film cast from THF. In the images, S is light grey, B dark grey (stained with OsO_4) and T appears white due to e -beam degradation. The red arrows in (b) mark the long period L_0 . c) The Lorentz corrected SAXS pattern depicts reflex positions typical for the gyroid morphology. The schematic in c) illustrates the arrangement of the blocks for the core-shell gyroid morphology: S = light grey, B = dark grey, T = green.

5. Conclusion

Bulk morphologies of 16 SBT triblock terpolymers were investigated *via* TEM and SAXS, and comprise: the core-shell cylinder (CYL), lamella–lamella (LL), undulated lamella or cylinder-in-lamella (CL) and core-shell gyroid (GYR) morphology. Whereas CYL, LL and GYR represent core-shell analogs of known diblock copolymer morphologies, the CL morphology is the result of merging shells of core-shell cylinders in a linear fashion. The rather simple phase behavior of SBT as compared to, *e.g.*, the more complex phase diagram of SBM, might be explained by comparing the χ -parameters of the participating blocks. Since the χ_{ST} as well as χ_{SB} is higher than χ_{BT} , a B/T interface is favored over S/T. To prevent the unfavorable S/T interface the B phase spreads onto T resulting in core-shell structures. Consequently, we observe

stability regions of the core-shell analogs of diblock copolymer morphologies over a broader range of block copolymer compositions, because the middle block plays only a minor role in structure evolution. The length of the S and T end blocks mostly determine the final morphology. On the one hand, the simple phase behavior of B reduces the number of possible morphologies to only a few, but on the other hand, it teaches us that proper combinations of χ -parameters (in multiblock copolymers) gives control over phase behavior with minor influence of block volume fractions. In view of applications, this example highlights the importance of knowledge of the block–block interactions, because morphologies that are challenging to target (*e.g.* gyroid) might become easier accessible by reducing the complexity of triblock terpolymer phase behavior through proper choice of monomers.

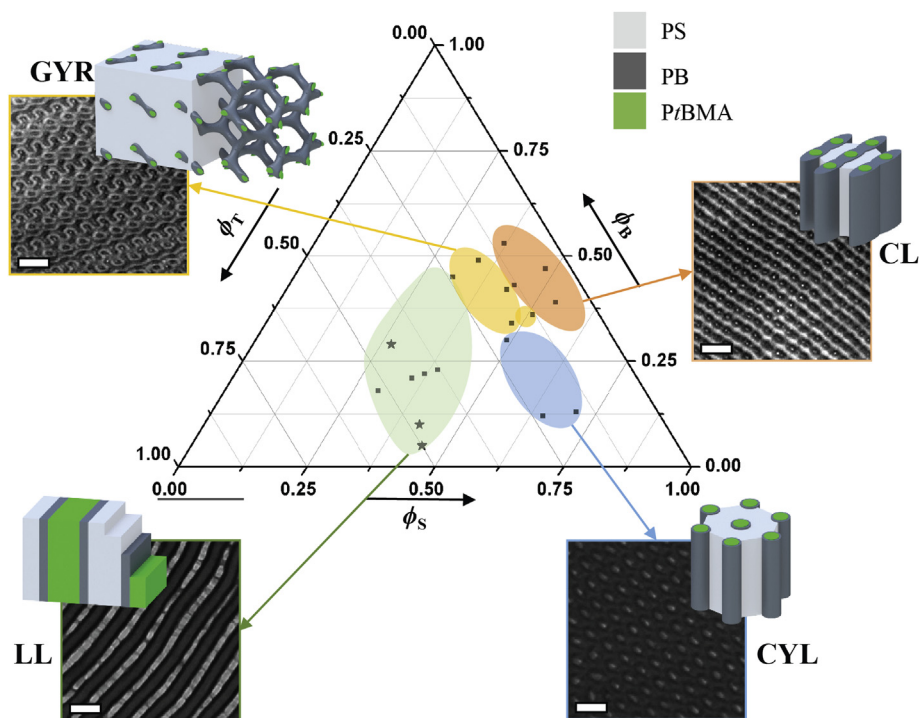


Fig. 7. Ternary phase diagram of SBT. The colored areas mark regions of the same morphology: blue: core-shell cylinder; green: lamella–lamella (stars denote literature values from Refs. [55,73]); orange: cylinder-in-lamella; yellow: core-shell gyroid. All phases are exemplified in TEM images with frames in corresponding colors. The scale bars are 100 nm.

Acknowledgements

The authors thank Annika Pfaffenberger for ultramicrotoming thin films. The authors acknowledge the Deutsche Forschungsgemeinschaft (DFG) for supporting this work within DFG Mu896/40-1 and SFB 840 (Project A2). This work was carried out under the Academy of Finland's Centre of Excellence Programme (2014–2019) and supported by ERC-2011-AdG (291364-MIMEFUN).

References

- Abetz V, Simon PFW. *Adv Polym Sci* 2005;189:125–212.
- Leibler L. *Macromolecules* 1980;13:1602–17.
- Matsen M, Schick M. *Phys Rev Lett* 1994;72:2660–3.
- Matsen MW, Bates FS. *Macromolecules* 1996;29:7641–4.
- Schmidt SC, Hillmyer MA. *J Polym Sci Part B Polym Phys* 2002;40:2364–76.
- Ryan AJ, Mai S-M, Patrick A, Fairclough J, Hamley IW, Booth C. *Phys Chem Chem Phys* 2001;3:2961–71.
- Khandpur AK, Förster S, Bates FS, Hamley IW, Ryan AJ, Bras W, et al. *Macromolecules* 1995;28:8796–806.
- Floudas G, Vazaiou B, Schipper F, Ulrich R, Wiesner U, Iatrou H, et al. *Macromolecules* 2001;34:2947–57.
- Hashimoto T, Tanaka H, Hasegawa H. *Macromolecules* 1990;23:4378–86.
- Abetz V, Goldacker T. *Macromol Rapid Commun* 2000;21:16–34.
- Warren SC, Messina LC, Slaughter LS, Kamperman M, Zhou Q, Gruner SM, et al. *Science* 2008;320:1748–52.
- Ruokolainen J, Mäkinen R, Torkkeli M, Mäkelä T, Serimaa R, ten Brinke G, et al. *Nat Mater* 2004;3:872–6.
- Ruokolainen J, ten Brinke G, Ikkala O. *Adv Mater* 1999;11:777–80.
- Valkama S, Kosonen H, Ruokolainen J, Haatainen T, Torkkeli M, Serimaa R, et al. *Nat Mater* 2004;3:872–6.
- Vukovic I, ten Brinke G, Loos K. *Macromolecules* 2012;45:9409–18.
- Kimishima K, Koga T, Hashimoto T. *Macromolecules* 2000;33:968–77.
- Shi L-Y, Hsieh I-F, Zhou Y, Yu X, Tian H-J, Pan Y, et al. *Macromolecules* 2012;45:9719–26.
- Fredrickson GH. *J Rheol* 1994;38:1045–67.
- Gupta VK, Krishnamoorti R, Chen Z-R, Kornfield JA, Smith SD, Satkowski MM, et al. *Macromolecules* 1996;29:875–84.
- Morkved T, Lu M, Urbas A, Ehrichs E, Jaeger H, Mansky P, et al. *Science* 1996;273:931–3.
- Schmidt K, Schorberth HG, Ruppel M, Zettl H, Hänsel H, Weiss TM, et al. *Nat Mater* 2008;7:142–5.
- Böker A, Elbs H, Hänsel H, Knoll A, Ludwigs S, Zettl H, et al. *Phys Rev Lett* 2002;89:135502.
- Bates FS, Fredrickson GH. *Phys Today* 1999;52:32–8.
- Ruzette A-V, Leibler L. *Nat Mater* 2005;4:19–31.
- Hückstädt H, Abetz V, Stadler R. *Macromol Rapid Commun* 1996;17:599–606.
- Hückstädt H, Göpfert A, Abetz V. *Macromol Chem Phys* 2000;201:296–307.
- Hadjichristidis N, Iatrou H, Pitsikalis M, Pispas S, Avgeropoulos A. *Prog Polym Sci* 2005;30:725–82.
- Hirao A, Matsuo Y, Oie T, Goseki R, Ishizone T, Sugiyama K, et al. *Macromolecules* 2011;44:6345–55.
- Hückstädt H, Göpfert A, Abetz V. *Polymer* 2000;41:9089–94.
- Müller AHE, Matyjaszewski K. *Controlled and living polymerizations*. Weinheim: Wiley-VCH; 2009.
- Stadler R, Auschra C, Beckmann J, Krappe U, Voigt-Martin I, Leibler L. *Macromolecules* 1995;28:3080–91.
- Zheng W, Wang Z. *Macromolecules* 1995;28:7215–23.
- Krappe U, Stadler R, Voigt-Martin I. *Macromolecules* 1995;28:4558–61.
- Breiner U, Krappe U, Abetz V, Stadler R. *Macromol Chem Phys* 1997;198:1051–83.
- Breiner U, Krappe U, Stadler R. *Macromol Rapid Commun* 1996;17:567–75.
- Tschierske C. *Non-conventional soft matter*. *Annu Rep Prog Chem Sect C* 2001;97:191–267.
- Ludwigs S, Böker A, Abetz V, Müller AHE, Krausch G. *Polymer* 2003;44:6815–23.
- Schacher F, Yuan J, Schorberth HG, Müller AHE. *Polymer* 2010;51:2021–32.
- Zhang K, Gao L, Chen Y. *Polymer* 2010;51:2809–17.
- Müllner M, Lunkenbein T, Miyajima N, Breu J, Müller AHE. *Small* 2012;8:2636–40.
- Lunkenbein T, Kamperman M, Li Z, Bojer C, Drechsler M, Förster S, et al. *J Am Chem Soc* 2012;134:12685–92.
- Darling SB. *Energy Environ Sci* 2009;2:1266–73.
- Hsueh H-Y, Chen H-Y, She M-S, Chen C-K, Ho R-M, Gwo S, et al. *Nano Lett* 2010;10:4994–5000.
- Orillall MC, Wiesner U. *Chem Soc Rev* 2011;40:520–35.
- Kim E, Vaynzof Y, Sepe A, Guldin S, Scherer M, Cunha P, et al. *Adv Funct Mater* 2014;24:863–72.
- Son JG, Gwyther J, Chang J-B, Berggren KK, Manners I, Ross CA. *Nano Lett* 2011;11:2849–55.
- Schacher FH, Rupar PA, Manners I. *Angew Chem Int Ed* 2012;51:2–25.
- Vukovic I, ten Brinke G, Loos K. *Polymer* 2013;54:2591–605.

- [49] Crossland EJW, Kamperman M, Nedelcu M, Ducati C, Wiesner U, Smilgies D-M, et al. *Nano Lett* 2009;9:2807–12.
- [50] Vukovic I, Punzhin S, Vukovic Z, Onck P, De Hosson JTM, ten Brinke G, et al. *ACS Nano* 2011;5:6339–48.
- [51] Du Sart GG, Vukovic I, Vukovic Z, Polushkin E, Hiekkataipale P, Ruokolainen J, et al. *Macromol Rapid Commun* 2011;32:366–70.
- [52] Li Z, Hur K, Sai H, Higuchi T, Takahara A, Jinnai H, et al. *Nat Commun* 2014;5:3247.
- [53] Erhardt R, Böker A, Zettl H, Kaya H, Pyckhout-Hintzen W, Krausch G, et al. *Macromolecules* 2001;34:1069–75.
- [54] Liu Y, Abetz V, Müller AHE. *Macromolecules* 2003;36:7894–8.
- [55] Walther A, André X, Drechsler M, Abetz V, Müller AHE. *J Am Chem Soc* 2007;129:6187–98.
- [56] Walther A, Müller AHE. *Chem Rev* 2013;113:5194–261.
- [57] Ruhland TM, Gröschel AH, Walther A, Müller AHE. *Langmuir* 2011;27:9807–14.
- [58] Ruhland TM, Gröschel AH, Ballard N, Skelton TS, Walther A, Müller AHE, et al. *Langmuir* 2013;29:1388–94.
- [59] Walther A, Hoffmann M, Müller AHE. *Angew Chem Int Ed* 2008;47:711–4.
- [60] Gröschel AH, Löbbling TI, Petrov PD, Müllner M, Kuttner C, Wieberger F, et al. *Angew Chem Int Ed* 2013;52:3602–6.
- [61] Walther A, Matussek K, Müller AHE. *ACS Nano* 2008;2:1167–78.
- [62] Bahrami R, Löbbling TI, Gröschel AH, Schmalz H, Müller AHE, Altstadt V. *ACS Nano* 2014;8:10048–56.
- [63] Schubert DW, Stamm M, Müller AHE. *Polym Eng Sci* 1999;39:1501–7.
- [64] Hanisch A, Gröschel AH, Förtsch M, Löbbling T, Schacher FH, Müller AHE. *Polymer* 2013;54:4528–37.
- [65] Goldacker T, Abetz V, Stadler R, Erukhimovich I, Leibler L. *Nature* 1999;398:137–9.
- [66] Schrage S, Sigel R, Schlaad H. *Macromolecules* 2003;36:1417–20.
- [67] Han D, Li X, Hong S, Jinnai H, Liu G. *Soft Matter* 2012;8:2144–51.
- [68] Williams DB, Carter BC. *Transmission electron microscopy*. Heidelberg: Springer; 2009.
- [69] Ah Toy A, Reinicke S, Müller AHE, Schmalz H. *Macromolecules* 2007;40:5241–4.
- [70] Lanzendörfer MG, Schmalz H, Abetz V, Müller AHE. In: Puskas JE, Storey R, editors. *In-situ spectroscopy of monomer and polymer synthesis*. New York/Dordrecht: Kluwer Academic/Plenum Publishers; 2002. p. 67–82.
- [71] Mark JE. *Physical properties of polymers handbook*. Woodbury: American Institute of Physics Press; 2007.
- [72] Sperschneider A, Hund M, Schoberth HG, Schacher FH, Tsarkova L, Müller AHE, et al. *ACS Nano* 2010;4:5609–16.
- [73] Abetz V, Markgraf K, Rebizant V. *Macromol Symp* 2002;177:139–45.
- [74] Neumann C, Loveday DR, Abetz V, Stadler R. *Macromolecules* 1998;31:2493–500.
- [75] Jiang S, Göpfert A, Abetz V. *Macromol Rapid Commun* 2003;24:932–7.
- [76] Hückstädt H, Goldacker T, Göpfert A, Abetz V. *Macromolecules* 2000;33:3757–61.
- [77] Hajduk DA, Harper PE, Gruner SM, Honeker CC, Kim G, Thomas EL, et al. *Macromolecules* 1994;27:4063–75.